
PADME: A Deep Learning-based Framework for Drug-Target Interaction Prediction

Qingyuan Feng¹, Evgenia Dueva², Artem Cherkasov^{2,3,*}, Martin Ester^{1,2,*}

1 School of Computing Science, Simon Fraser University, 8888 University Drive, Burnaby, BC, V5A1S6, Canada

2 Vancouver Prostate Centre, Vancouver, BC V6H3Z6, Canada

3 Department of Urologic Sciences, University of British Columbia, Vancouver, BC, Canada

* ester@sfu.ca; artc@interchange.ubc.ca

Abstract

In silico drug-target interaction (DTI) prediction is an important and challenging problem in biomedical research with a huge potential benefit to the pharmaceutical industry and patients. Most existing methods for DTI prediction including deep learning models generally have binary endpoints, which could be an oversimplification of the problem, and those methods are typically unable to handle cold-target problems, i.e., problems involving target protein that never appeared in the training set. Towards this, we contrived PADME (Protein And Drug Molecule interaction prEdiction), a framework based on Deep Neural Networks, to predict real-valued interaction strength between compounds and proteins. PADME takes both compound and protein information as inputs, so it is capable of solving cold-target (and cold-drug) problems. To our knowledge, we are the first to combine Molecular Graph Convolution (MGC) for compound featurization with protein descriptors for DTI prediction. We used multiple cross-validation split schemes and evaluation metrics to measure the performance of PADME on multiple datasets, including the ToxCast dataset, which we believe should be a standard benchmark for DTI problems, and PADME consistently dominates baseline methods. The results of a case study, which predicts the interactions between various compounds and androgen receptor (AR), suggest PADME's potential in drug development. The scalability of PADME is another advantage in the age of Big Data.

1 Introduction

Finding out the interaction strengths between compounds (candidate drugs) and target proteins is of crucial importance in the drug development process. However, it is both expensive and time-consuming to be done in wet lab experiments, while virtual screening using computational (also called "*in silico*") methods to predict the interactions between compounds and target proteins can greatly accelerate the drug development process at a

significantly reduced cost. Indeed, machine learning models for drug-target interaction (DTI) prediction are often used in computer-aided drug design [5].

Datasets often used for training and evaluating machine learning models for DTI prediction include observations of compounds interacting with enzymes, ion channels, nuclear receptors, etc [40]. These datasets contain binary labels for the interaction of certain drug-target pairs, with 1 indicating a known interaction. Recently, the community has also explored the usage of datasets with real-valued interaction strength measurements [9, 22], which include the Davis dataset [4] that uses the inhibition constant (K_i), the Metz dataset [18] that uses the dissociation constant (K_d) and the KIBA dataset [31] whose authors devised their own measurement index.

Existing traditional machine learning methods for predicting DTI can be roughly divided into similarity-based and feature-based approaches. Similarity-based methods depend on the assumption that compounds with similar structures should have similar effects. Feature-based methods construct feature vectors as input, which are generated by combining descriptors of compounds with descriptors of targets, and the feature vectors serve as inputs of algorithms like SVM [9]. Existing traditional machine learning methods for predicting DTI can be roughly divided into similarity-based and feature-based approaches, and most of them formulate the problem as a classification problem. Similarity-based methods depend on the assumption that compounds with similar structures should have similar effects. Feature-based methods construct feature vectors as input, which are generated by combining descriptors of compounds with descriptors of targets, and the feature vectors serve as inputs for algorithms such as support vector machine (SVM) [9].

SimBoost [9] and KronRLS [22] are two state-of-the-art methods for DTI prediction. Both of them have single outputs. KronRLS is based on Regularized Least Squares and utilizes the similarity matrices for drugs and targets to get the parameter values. SimBoost is a feature-based method, but in its feature construction, similarity matrices of the drugs and targets are also involved. These methods can both predict continuous values and binarized values. However, these methods either simply rely on similarities, or require expert knowledge to define the relevant features of proteins and compounds. Additionally, they are unable to model highly complex interactions within compound molecules [17] and between the compounds and their target proteins.

Deep Neural Networks (DNN) promise to address these challenges.

Deep learning, the machine learning method based on DNN, has been enjoying an ever-rising popularity in the past few years. It has seen wide and exciting applications in computer vision, speech recognition, natural language processing, reinforcement learning, and drug-target interaction prediction. DNNs can automatically extract important features from the input data, synthesize and integrate low-level features into high-level features, and capture complicated nonlinear relationships in a dataset [15, 25]. Deep learning-based DTI prediction has been shown to consistently outperform the existing methods and has become the new "golden standard" [3, 16, 32].

The current deep learning approaches to drug-target interaction prediction can be roughly categorized based on their neural network types and prediction endpoints. Simple feedforward neural networks, Convolutional Neural Networks (CNN) and Recurrent Neural Networks (RNN) have been adopted in various papers [42]. To our knowledge, all existing deep learning methods, except those that have 3D structural information as input, treat the problem as a classification problem, most of which are binary, namely active/inactive.

Though there are deep learning models using 3D structural information that yield good results in regression problems [7, 36], the requirement of 3D structural information limits the applicability of a model since such information is not always available, so we do not consider them in this paper. As deep learning for DTI is still in its infancy, the current models have several disadvantages.

First, formulating the problem as a classification problem has several disadvantages: obviously, the classification result depends on a predefined binarization threshold, which introduces some arbitrariness into the data; some useful information is lost, for instance, true-negative and missing values may not be discriminated [9, 22]. On the other hand, if we formulate it as a regression problem, not only can we avoid the problems above, but given the regression results, the real-valued outputs can be easily converted to produce a ranking or classification. Some existing non-DNN methods formulate the problem as a regression problem, in which the interaction strength between the drug molecule and the target protein is a real number, serving as the regression target [9]. Common real-valued interaction strength metrics K_i, K_d , 50% inhibition concentration (IC_{50}), etc.

The second problem is that most of the existing deep learning methods do not incorporate the target protein information into the network, except very few recent works, like Wen et al. [37]. As a result, the models are unable to solve the "cold target" problem, i.e. to predict the drug-target interactions for target proteins absent in the training dataset.

DeepDTI [37] addressed the second problem by combining the protein information with the compound feature vector. It uses the classical Extended-Connectivity Fingerprint (ECFP) [24] for describing compounds, which relies on a fixed hashing function and cannot adjust to specific problems at hand. DeepDTI concatenates ECFP and Protein Sequence Composition (PSC) descriptors [2] (describing the target proteins' sequence information) to construct a feature vector, which is fed into a Deep Belief Network (DBN) to predict a binary endpoint. DeepDTI outperformed the state-of-the-art methods on a dataset extracted from DrugBank.

In this paper, we propose PADME (Protein And Drug Molecule interaction prEdiction), a deep learning-based framework for predicting DTI. PADME overcomes the limitations of the existing methods by predicting real-valued interaction strengths instead of binary class labels, and, to address the cold-start problems (drugs or targets that are absent from the training set but appear in the test set), PADME utilizes a combination of drug and target protein features/fingerprints as the input vector. Because the DBN used in DeepDTI has fallen out of favor in the deep learning community after Rectified Linear Units (ReLU) were introduced to improve the performance of feedforward networks, PADME uses a feedforward network to connect the input vector to the output layer. PADME adopts Molecular Graph Convolution (MGC) which is more flexible than ECFP, because it learns the mapping function from molecular graph representations to feature vectors [1, 6, 12]. Similar to DeepDTI, we used Protein Sequence Composition (PSC) descriptor to represent the protein. To the best of our knowledge, this work is the first to integrate MGC with protein descriptors for the DTI problem. In addition to the kinase inhibitor datasets used by previous researchers, we also use the ToxCast dataset [33], and we believe this large high-quality dataset, with its much larger variety of proteins, could be another useful benchmarking dataset for future researches.

We conducted computational experiments with multiple cross-validation settings and evaluation metrics. The results demonstrated the superiority of PADME over baseline

methods across all experimental settings. Besides, PADME is much more scalable than SimBoost and KronRLS since it does not rely on similarity matrices and can accommodate multiple outputs. As a case study, we also applied PADME to predict the interaction strength between some compounds and the androgen receptor (AR). We examined the top 100 compounds predicted to have strong antagonist effects on AR and found that they are biologically/chemically meaningful, suggesting that the predictions of PADME have practical implications.

The subsequent sections of the paper are organized as follows. The Method section will introduce the methods for compound featurization, protein featurization, and network structure. The Experiments section will present the experiments conducted, introducing the baseline methods, datasets used, experimental design, and the experimental results. The Discussion section clarifies some implementation and design choices, and outlines possible future directions to further this work. The last section concludes the whole paper.

2 Method

PADME is a deep learning-based DTI prediction model which combines the small-molecule compound (candidate drug) and target protein feature vectors. We consider two variants of PADME with either Molecular Graph Convolution (MGC) or ECFP [24] as the compound featurization method. MGC [6, 12] is an extension of Convolutional Neural Network which learns a vector representing the compound from the graph-based representation of the molecule. In the graph representation of molecules, the atoms are denoted by nodes, while the bonds are denoted by edges. For the protein, we use Protein Sequence Composition (PSC) descriptor [2]. In fact, PADME is compatible with all kinds of protein descriptors and molecular featurization methods. The compound vector is concatenated with a target protein vector to form the Combined Input Vector (CIV) for the neural network. PADME predicts a real-valued interaction strength, i.e., it solves a DTI regression problem. The structure of the network is shown in Figure 1: if we use the molecular graph convolutional network to get the molecular vector, that network will be trained together with the feedforward network connecting the CIV to the prediction endpoint in an end-to-end fashion.

2.1 Compound Featurization

There has been a lot of research on representing small molecules (compounds) as a descriptor or fingerprint. Among the traditional molecular descriptors and fingerprints, ECFP [24] is widely adopted as the state-of-the-art method for compound featurization [6], and was also used in DeepDTI [37]. However, it has a fixed set of mapping and hashing functions, unable to be tailored for the specific task at hand.

DNN, especially MGC, can be used to generate more flexible feature vectors. Instead of depending only on the molecule, compound feature vectors generated using DNN depend on both the molecule and the prediction task (Boolean or continuous). DNN-derived feature vectors can outperform the ECFP baseline and at times offer some good interpretability [1, 6, 42]. The MGC takes into account the neighbors of a node when computing the intermediate feature vector for a specific node, and the same operation is applied to the neighborhood of each node (atom), hence it is analogous to ordinary convolutional

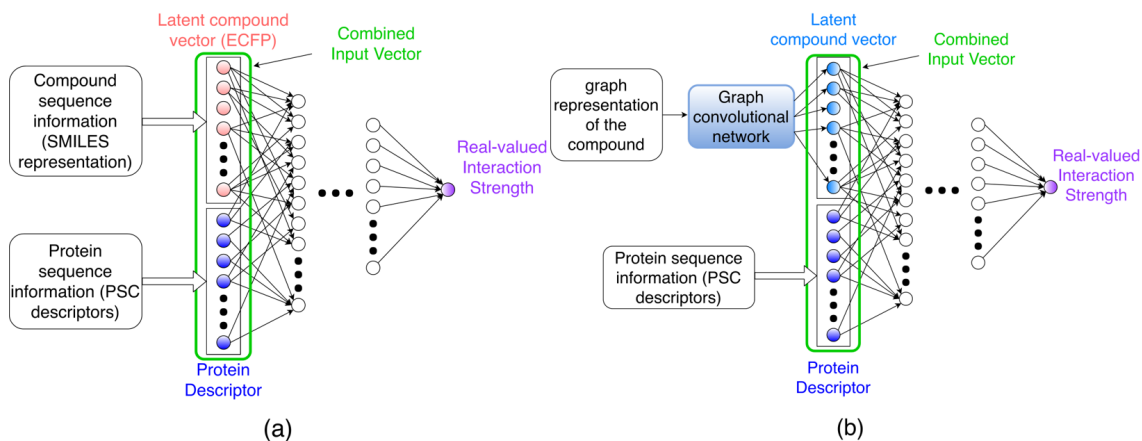


Figure 1. a) **PADME-ECFP architecture.** The Extended-Connectivity Fingerprint was used as the molecular input to the model. b) **PADME-GraphConv architecture.** Note that the graph convolutional network generating the latent molecular vector is trained together with the rest of the network, while the protein descriptor generation process is independent from the training of the network. The black dots represent omitted neurons and layers.

networks typically used in Computer Vision [6, 8]. Due to the GraphConv model [39] among MGC models being more recent and popular with an easier implementation, we use the GraphConv model as a representative of MGC under the time and resource constraints.

We applied both types of compound featurization methods: ECFP and GraphConv, and compared their performance.

2.2 Target Protein Featurization

There exist many schemes to represent the target protein as a feature vector based on its amino acid sequence information. DeepDTI [37] used Protein Sequence Composition (PSC) descriptor, which has 8420 entries for each protein, consisting of amino acid composition (AAC), dipeptide composition (DC), and tripeptide composition (TC) [2]. It captures rich information and does not transform the protein as much as some other protein descriptors (which implies less human knowledge required and less information loss), which we think could be a desirable attribute for being the input to a neural network. In addition to the 8420 entries for each protein sequence, we added an additional binary entry signaling the phosphorylation status so that the Davis dataset (see below) can be represented more accurately, with '1' denoting phosphorylated, resulting in 8421 entries in total.

Mousavian et al. [20] used PSSM (Position Specific Scoring Matrix) descriptor to represent the protein, which focuses on dipeptide sequences and is related to the evolutionary history of proteins [27]. It is observed that PSSM performed pretty well. Other popular protein sequence descriptors include Autocorrelation, CTD (Composition, Transition and Distribution) descriptor, Quasi-sequence order, etc [2].

As PSC contains rich information (like tri-peptide sequence occurrence) with high dimensionality, and has already shown promising performance in deep learning-based models for DTI prediction [37], we use PSC in this research. There could be future comparisons of the performance of PSC and other protein featurization methods as an

extension to this work.

2.3 Architecture of the Deep Neural Network

PADME uses a feedforward neural network taking the CIV as the input. The PADME architecture has one output neuron per prediction endpoint, i.e., one output neuron for most datasets, and 61 output neurons for the ToxCast dataset (see below). DNNs with single output neuron are called single-task networks, and those with multiple output neurons are called multi-task networks. Although we only consider the DTI regression problem in this paper, PADME can also be used for constructing classification models with minimal changes, either by binarizing the continuous prediction results or by directly using a softmax/sigmoid layer as the output layer, of which the latter could be more preferable.

For regularization, we use Early Stopping, Dropout and Batch Normalization techniques [8]. Hyperparameters like dropout rates are automatically searched to find the best set of them before running cross-validation, as elaborated in the “Experimental Design” section. The Adam optimizer [13] was used to train the network. The activation functions used for fully connected layers are all Rectified Linear Units (ReLU).

3 Experiments

3.1 Baseline methods

There are two baseline methods used as comparisons: SimBoost [9] and KronRLS [22], which are state-of-the-art methods for the DTI regression task.

SimBoost Simboost predicts continuous DTI values using gradient boosting regression trees. Each drug-target pair corresponds to a continuous DTI value, and the authors defined 3 types of features to characterize the drug-target pairs: type 1 features for individual entities (drugs or targets); type 2 features, derived from the drug similarity networks and target similarity networks; type 3 features, which are derived from drug-target interaction network. The 3 types of features are concatenated to form a feature vector.

Let $x_i \in R^d$ denote the vector of features for the i -th drug-target pair, while $x_i \in R$ is its binding affinity. The score \hat{y}_i predicted for input x_i is computed as follows:

$$\hat{y}_i = \phi(x_i) = \sum_{k=1}^K f_k(x_i), f_k \in F$$

where K is the number of regression trees and F is the space of possible trees. To learn the set of trees f_k , they defined a regularized objective function:

$$L(\phi) = \sum_i l(\hat{y}_i, y_i) + \sum_k \Omega(f_k)$$

where l is a loss function that evaluates the prediction error, Ω is a function that penalizes overfitting. The model is trained additively: for each iteration t , the tree space F is searched to find a new tree f_t that optimizes the objective function, which is added to the ensemble afterwards. Trees that optimize $L^{(t)}$ are iteratively added to the model for a number of pre-specified iterations.

SimBoost cannot handle cold-start problems, which means it does not work for pairs in the test set with a drug or target that is absent from the training set.

KronRLS KronRLS stands for Kronecker Regularized Least Squares. It learns a prediction function $f(x)$ for drug-target pairs. It could use some similarity measure between two drug-target pairs x and x_i , and $f(x)$ is constructed as a linear combination of the similarity values. The algorithm learns the coefficients of this linear combination from the training data.

Unlike SimBoost, KronRLS is applicable to cold-start problems.

3.2 Datasets and tools

Similar to He et al. [9], we used kinase inhibitor datasets. Following its naming convention, we call them Davis dataset [4], Metz dataset [18] and KIBA dataset [31], respectively. However, the versions of these datasets curated by Pahikkala et al. [22] that He et al. [9] used was slightly different from the original dataset, and Pahikkala et al. did not give the corresponding justifications. We thus used the data provided by the respective original authors, then preprocessed them ourselves as described in the Supporting Information. We assume the observations within each dataset are under the same experimental settings. Metz dataset contained lots of imprecise values, which we discarded in the preprocessing step.

Because of the limitations of SimBoost and KronRLS, we filtered the datasets. The original KIBA dataset contains 52498 compounds, a large proportion of which only have the interaction values with very few proteins. Considering the huge compound similarity matrix required and the time-consuming matrix factorization used in SimBoost, it would be infeasible to work directly on the original KIBA dataset. Thus, we had to filter it rather aggressively so that the size becomes more manageable. This suggests that PADME, which does not require drug-drug or target-target similarity matrices or matrix factorization, is much more scalable than KronRLS and SimBoost, both of which have at least $O(n^2)$ time and space complexity. We chose to use a threshold of 6 (drugs and targets with no more than 6 observations are removed), more lenient than the threshold of 10 used in He et al. [9], aiming at a reduction of the unfair advantages that SimBoost can gain by keeping only the denser submatrix of the interaction matrix.

For the Metz and Davis datasets, as SimBoost cannot handle cold drug/target problem, we had to ensure that in creating Cross-Validation folds, each drug or target appear in at least 2 folds, thus those drugs/targets with no more than 1 observation are discarded.

We also used the ToxCast dataset [33], containing a much larger variety of proteins [34]. It contains toxicology data obtained from high-throughput *in vitro* screening of chemicals. The prepared dataset (see Supporting Information) contains observations for 530605 drug-target pairs. Its large size and coverage of diverse protein types allows us to test the robustness and scalability of computational models for DTI prediction. Because it contains lots of heterogeneous endpoints, we manually divided those endpoints into 61 different measurements for interaction strength based on assay type, such that observations in each measurement are homogeneous. The number of observations in each measurement range from 290 to 160,000. For the ToxCast dataset, we constructed multi-task networks, in which each measurement corresponds to a neuron in the output layer. As KronRLS and

SimBoost are both single-task models, to evaluate the performance of those two models on the ToxCast dataset, one must train 61 models for each of them, which would be an extraordinarily tedious job, so we did not run the SimBoost and KronRLS models on ToxCast. This indicates PADME is not only more scalable in the number of drugs/targets, but also much more scalable in the number of endpoints, since it can have multiple outputs in one model. As ToxCast does not have the bottlenecks imposed by KronRLS and SimBoost, we did not filter it.

Please refer to table 1 for the sizes of the datasets after filtering.

Table 1. Dataset sizes after filtering.

Dataset	Number of drugs (compounds)	Number of target proteins	Total number of drug-target pairs used
Davis	72	442	31824
Metz	1423	170	35259
KIBA	3807	408	160296
ToxCast (No filtering)	7657	335	530605

We applied the same numerical transformation as He et al. [9] to the datasets: $transformed = 4 - \log_{10}(original)$. For the ToxCast dataset, we changed the inactive value from 1,000,000 to 1,000, so that there would be no large gaps in the distribution after transforming the data.

The model was constructed based on the implementation of the DeepChem python package, in which RDKit [14] was used; the networks were constructed using TensorFlow 1.3. In the practical application, PADME takes SMILES representations of the candidate drug as part of the input, which are transformed into graph representations or ECFP by the program. PSC was obtained independently from this process: we used the propy python package [2] to generate PSC descriptors, and manually added a binary entry indicating phosphorylation. Afterwards, PSC was saved in a standalone file, which the program reads into the memory in the runtime.

The experiments were conducted on a Linux server with 8 Nvidia Geforce GTX 1080Ti graphics cards, among which 4 were used. The server has 40 logical CPU cores and 256 GB of RAM. A computer with less than 110 GB RAM might not be able to perform cross-validation for the ToxCast dataset using GraphConv-based PADME.

3.3 Experimental Design

To examine PADME’s prediction power, we used cross-validation (CV). To measure the performance of the model under different settings, multiple CV splitting schemes were employed to evaluate the predictions of the models trained from the training sets against the known interaction strengths in the test sets. The performances of PADME-ECFP and PADME-GraphConv were compared against each other under identical settings.

We performed 5-fold CV, for which every compound or target must be present in at least 2 folds for SimBoost to work. There are no such restrictions for KronRLS, since it can handle cold-start data. As cold-start prediction is an important objective in DTI prediction (and an advantage of PADME), we also included cold-splitting in constructing

the cross-validation folds, such that all compounds (candidate drugs) in the test fold are absent from the training fold (cold-drug split), or all targets in the test fold are absent from the training fold (cold-target split). The third splitting method is called "warm split" in this paper, in which every drug or target appears in at least 2 folds. As we did not run SimBoost on ToxCast data, there is no need to perform warm-split on it, we then used random split in that case (if we force a warm split on ToxCast dataset, a filter threshold of 1 must be used to reduce the size of the dataset, which is undesirable). Though Pahikkala et al. [22] suggested another splitting scheme which results in simultaneous cold-drug and cold-target in each validation fold, as it greatly decreases the size of the training set in each fold (4/9 of the original data instead of 4/5 in other splitting schemes), we decided that it would cause unfair comparison and did not use it.

For every dataset, we performed three types of CV splitting (warm, cold-target, cold-drug), and for every CV splitting scheme, we calculated the prediction errors of the applicable models (KronRLS and PADME for all splitting schemes, SimBoost for warm splits only). To reduce the random effects, we repeated the splitting several times for each splitting scheme on Davis, Metz and KIBA datasets and calculated the average values of the evaluation metrics of the prediction results across the splits. For the Davis and Metz datasets, we repeated 3 splits for each splitting scheme; for the KIBA dataset, we did 2 for each, as it is a much bigger dataset; for the ToxCast dataset, the largest one, we only did 1 split for each scheme.

Not only do we have multiple splitting methods, we also used multiple model settings and evaluation metrics. For each of PADME-ECFP and PADME-GraphConv, a single-task network was trained for every splitting scheme of every dataset, except ToxCast, for which we constructed a multi-task network with 61 output neurons to avoid the complexity resulting from 61 separate single-task networks.

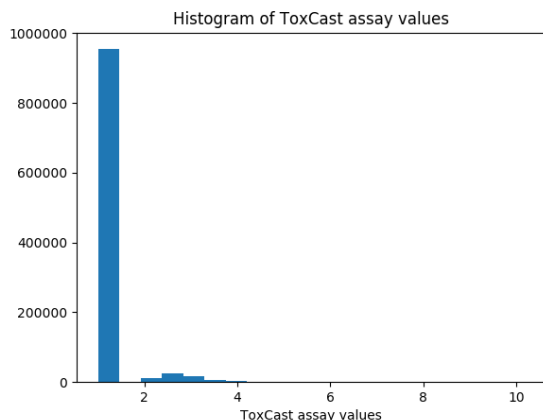
We also wanted to investigate whether PADME can predict the ordering of the interaction strengths correctly, so in addition to metrics focusing on value correctness (RMSE (Root Mean Squared Error) and R^2), we also used metrics focusing on order correctness, like concordance index (CI). Using CI as a metric in cheminformatics setting was proposed by Pahikkala et al. [22]. It measures the probability of correctly ordering the non-equal pairs in the dataset, ranging across [0, 1], with bigger values indicating better results. If you use the same value (e.g. mean value of the training set) as the predicted results across the test set, the CI would be 0.5.

To improve the readability of the reported results for ToxCast dataset, the performance metrics are averaged across the 61 different measurements, weighted by their number of observations, so the results reported for the ToxCast dataset look the same as other datasets with single endpoints.

As an exploratory analysis of the datasets, we found the ToxCast to be special. As shown in Figure 2, the transformed ToxCast dataset is extremely concentrated at a value of 1 which corresponds to no interaction. This led us to ignore the R^2 values for this dataset: because R^2 is sensitive to the overall departure of the predicted values from the true values, we argue that the huge concentration of values has rendered R^2 uninformative in measuring the performance of the model on the ToxCast dataset. This concentration of values also makes RMSE less informative than it otherwise would be (since one can blindly guess inactive values for all and still get pretty good RMSE), so we argue that CI is the most useful metric in the ToxCast dataset prediction evaluation. This strong imbalance

in the dataset caused us to consider balancing it through oversampling (see supporting information).

Figure 2. The histogram of the distribution of the negative log transformed ToxCast measurement results. The majority (over 94%) are concentrated at one inactive value.



store one optimal set of hyperparameters per $(dataset, PADME\ variant)$ pair, which were then used for all CV settings for that $(dataset, PADME\ variant)$ pair. Note that, for simplicity and to examine the robustness of PADME, the set of hyperparameters found in the random splitting was used in all CV settings, including those with cold-drug split and cold-target split, though we believe better CV results could be achieved if the hyperparameter searching processes are specifically designed for that CV fold split scheme, e.g., for cold-target CV folds, we could use the hyperparameters found by running the Bayesian Optimization on cold-target splitted datasets.

The resulting networks typically have 2 or 3 fully-connected layers connecting the CIV to the output unit, with thousands of neurons in each of the layers. Each fully-connected layer is batch-normalized.

3.4 Experimental Results

3.4.1 Quantitative Results

The good performance of PADME is confirmed by the quantitative experimental results. In the results listed in tables 2 to 4, the bold numbers indicate the best values attained for each setting. We can see that the two versions of PADME dominate the other methods¹, with the only exception of SimBoost outperforming PADME-GraphConv on Metz dataset. We think it could be due to the small dataset size: PADME-GraphConv could be underfitting for Metz data, while SimBoost uses gradient boosting trees, a machine learning model better suited at small dataset than Deep Neural Networks. Because it does not use MGC, PADME-ECFP has a much smaller network than PADME-GraphConv, so we think the former does not suffer from underfitting as seriously on Metz dataset. However, we do not observe the same phenomenon on Davis dataset, which has a similar size and even fewer

¹Note that the SimBoost results reported here are considerably worse than the results reported in their original paper. It is because we have examined their source code and found they calculated MSE but reported it as RMSE.

entities.

It is somewhat surprising that PADME-ECFP is not outperformed by PADME-GraphConv; instead, it slightly outperforms PADME-GraphConv in many cases, though in general their performances are almost indistinguishable from each other. PADME-ECFP only takes about 23% of the time and 45% the space (RAM) of PADME-GraphConv in the training process and yields similar (and sometimes better) results, so PADME-ECFP is a more reasonable choice. Nonetheless, we cannot be certain that PADME-GraphConv and PADME-ECFP truly have similar performance, as there might be a better set of hyperparameters for each model that would differentiate their performances significantly. Though our results demonstrate the power of ECFP, future researchers should continue investigating MGC.

Table 2. The performance of regression across different datasets measured in RMSE (smaller is better)

Dataset	Cross Validation Splitting type	RMSE			
		PADME-ECFP	PADME-GraphConv	SimBoost	KronRLS
Davis	warm	0.432191	0.432245	0.481973	0.572941
	Cold Drug	0.785358	0.806446	NA	0.840484
	Cold Target	0.560054	0.578407	NA	0.659645
Metz	warm	0.552927	0.59926	0.581254	0.781284
	Cold Drug	0.711698	0.742916	NA	0.784291
	Cold Target	0.791535	0.818935	NA	0.898888
KIBA	warm	0.432138	0.418691	0.468883	0.656647
	Cold Drug	0.602012	0.620291	NA	0.702427
	Cold Target	0.616767	0.623449	NA	0.681109
ToxCast	warm(random)	0.405633	0.407789	NA	NA
	Cold Drug	0.444847	0.445019	NA	NA
	Cold Target	0.486978	0.494392	NA	NA

From tables 2 to 4 we can observe an interesting phenomenon: when there are many compounds and few targets in the training set, the cold-drug predictions tend to outperform the cold-target predictions; on the other hand, when there are many targets and few compounds, the cold-target predictions tend to be better than the cold-drug ones. We hypothesize that it is because the models can be more robust in entities (drugs or targets) with more information diversity in the training set, thus performing better in the corresponding scenario. This trend is not only present in the PADME models, but in KronRLS as well. It seems that the models also require much more types of compounds than proteins for learning their chemical features, as can be seen from the KIBA dataset, whose cold-drug and cold-target performances are very similar, though it has 3807 compounds and only 408 proteins. And, as expected, there is a universal trend that the performance of warm splits is always better than that of cold-drug or cold-target splits.

The fact that PADME outperforms both SimBoost and KronRLS demonstrates the power of DNN to learn complicated nonlinear relationships between drug-target pairs and interaction strength. Furthermore, the results presented might be an understatement of the real performance of PADME in cold-drug and cold-target scenarios, as the training

Table 3. The regression accuracy on the different datasets measured in Concordance Index. (larger is better)

Dataset	Cross Validation Splitting type	Concordance Index			
		PADME-ECFP	PADME-GraphConv	SimBoost	KronRLS
Davis	warm	0.903882	0.903892	0.887096	0.87578
	Cold Drug	0.716298	0.720008	NA	0.692436
	Cold Target	0.855025	0.844831	NA	0.80751
Metz	warm	0.807563	0.794003	0.794381	0.748522
	Cold Drug	0.742403	0.741041	NA	0.709156
	Cold Target	0.698305	0.707959	NA	0.647
KIBA	warm	0.857452	0.863699	0.840456	0.783103
	Cold Drug	0.773099	0.754999	NA	0.688972
	Cold Target	0.771671	0.767902	NA	0.7122
ToxCast	warm(random)	0.796547	0.798712	NA	NA
	Cold Drug	0.720573	0.72858	NA	NA
	Cold Target	0.684814	0.690501	NA	NA

Table 4. The performance of regression across different datasets measured in R^2 (larger is better)

Dataset	Cross Validation Splitting type	R^2			
		PADME-ECFP	PADME-GraphConv	SimBoost	KronRLS
Davis	warm	0.760728	0.76099	0.703138	0.580148
	Cold Drug	0.191118	0.115659	NA	0.047802
	Cold Target	0.594517	0.569119	NA	0.439302
Metz	warm	0.667115	0.608763	0.632297	0.335489
	Cold Drug	0.446423	0.395589	NA	0.328515
	Cold Target	0.31438	0.267742	NA	0.11295
KIBA	warm	0.745663	0.761212	0.700674	0.412822
	Cold Drug	0.5058	0.472761	NA	0.326592
	Cold Target	0.479066	0.467213	NA	0.363054
ToxCast ^a	warm(random)	NA	NA	NA	NA
	Cold Drug	NA	NA	NA	NA
	Cold Target	NA	NA	NA	NA

^a We did not report R^2 for ToxCast because of its imbalanced nature.

and validation sets for hyperparameter searching are randomly split, resulting in a set of hyperparameters that suit well for randomly split CV folds, but perhaps not for cold-drug and cold-target folds. This deliberately unfair comparison shows the robustness of the PADME models.

3.4.2 Qualitative Results

For qualitative results we used plots to visualize the prediction performance.

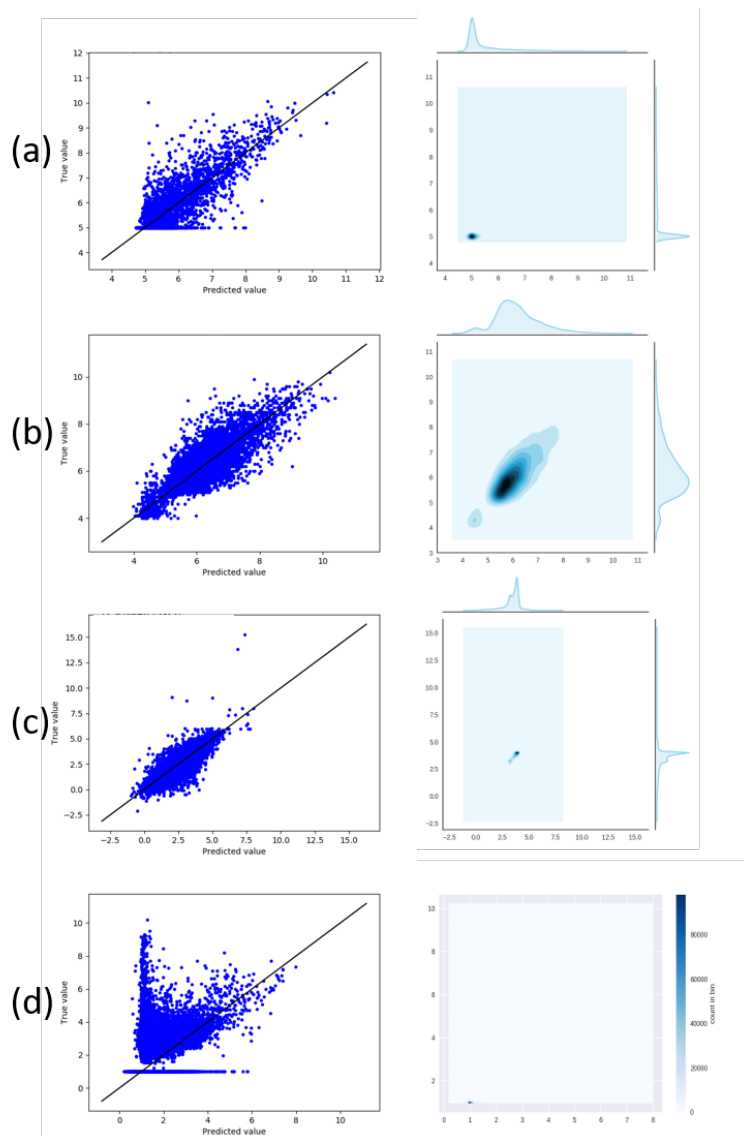
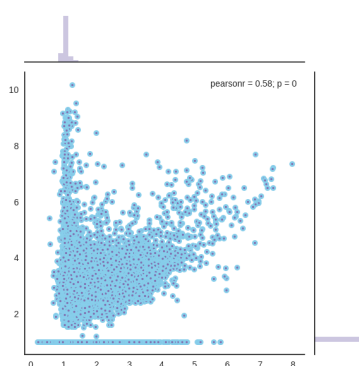


Figure 3. Scatter plot and contour plot of predicted VS true values across all datasets. The panels **a**, **b**, **c** and **d** correspond to **Davis**, **Metz**, **Kiba** and **ToxCast** datasets, respectively. The axes in the two plots of the same panel are the same, and both plots are generated from the same data. The diagonal lines in the scatter plots are the reference lines where $predicted = true\ value$.

We also present the plots of the predicted values (by PADME-ECFP) VS true values for each dataset, as can be seen in Figure 3. For each panel in the figure, there is a scatter plot, and a contour plot (the darkness of the color represents density of data points) with univariate density curves on the margins. Both plots in each figure are plotted from the exact same data. Figure 3(d) is an exception, it includes a hexagon plot instead of a contour plot, because the contour plot fails to show anything (but the density curves on the margins are plotted), possibly because the data points of ToxCast are too concentrated to be shown correctly on the contour plot, as can be observed from the hexagon plot. To

Figure 4. ToxCast data scatter plot with marginal histograms, generated from the same data as Figure 3(d)



help visualize ToxCast better, we added a Figure 4 which is a scatter plot of the same data as Figure 3(d), with histograms on the margins. Clearly, all datasets except Metz data are very concentrated at some values.

Because the concentration of Davis and ToxCast datasets pose problems in visualizing the prediction performances on them, we decided to plot the scatter plots and contour plots of the true active and true inactive data points separately for those datasets (figures 5 and 6). We can see the Davis data was predicted pretty well on both true active and inactive values, while ToxCast data was strongly influenced by inactive values and the prediction performance was not very good.

To tackle the imbalanced dataset problem in ToxCast, we tried to train a model on oversampled dataset and measured its performances. Please refer to the Supporting Information.

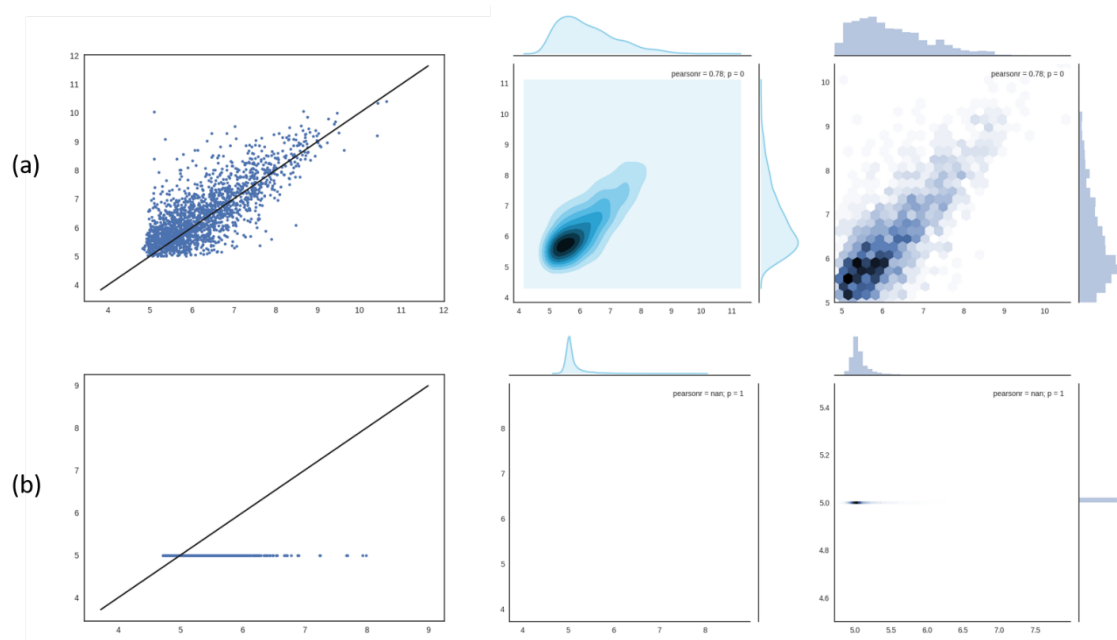


Figure 5. Plots for Davis dataset predicted value VS true value. Panel (a) corresponds to the true active values, while panel (b) corresponds to true inactive values. Similar to figure 3, all plots in the same panel are plotted from the same data.

3.4.3 Case Study

In addition to the quantitative and qualitative evaluations shown above, we performed a case study to further validate the predictions of PADME by investigating the compounds predicted to interact strongly with selected target proteins.

In our case studies we focused on the androgen receptor (AR), for which alterations of functions are associated with prostate [41] and breast cancers [19].

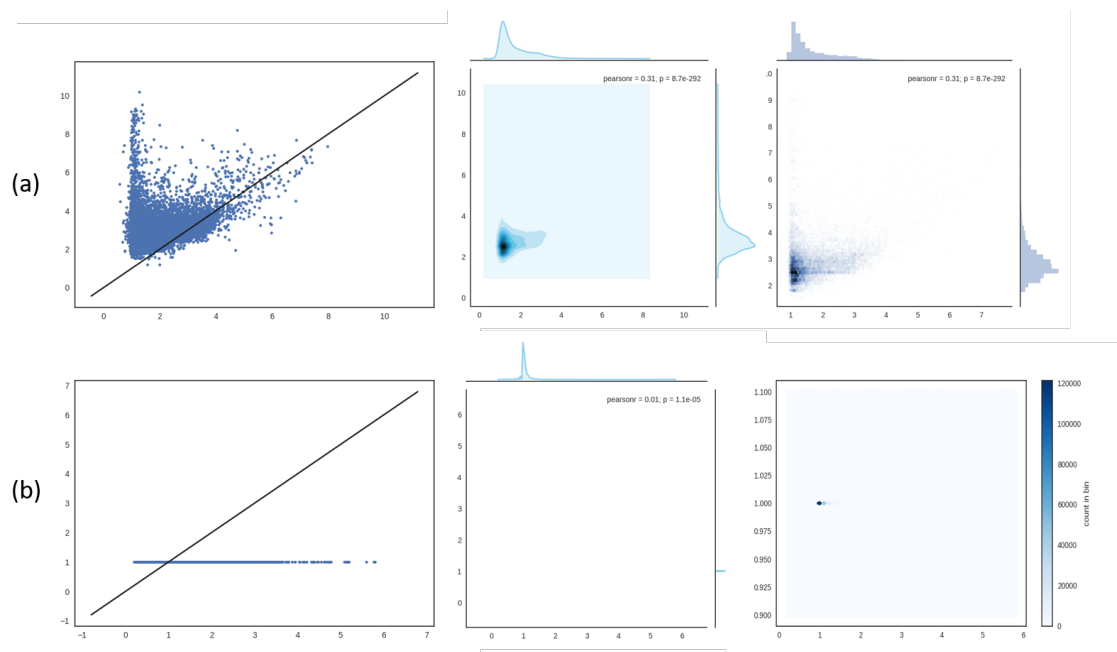


Figure 6. Similar to Figure 5, plots for ToxCast dataset. Panel (b) uses a different hexagon plot from (a), because that form of hexagon plot on panel (b) does not show properly.

We used all compounds in the datasets used in this paper, together with all the compounds in US National Cancer Institute human tumour cell line anticancer drug screen data (NCI60), and AR as the only target protein. NCI60 dataset records the in vitro drug response of cancer cell lines [28]. For prediction, we used both PADME models trained on ToxCast random-split CV folds, then took the average of the predictions made by PADME-ECFP and PADME-GraphConv. The reason we chose ToxCast is that it has the most diverse set of compounds and proteins. Because there are 61 outputs in PADME models trained on ToxCast data, we had to propose a set of coefficients to calculate a composite AR antagonist score (details in the Supporting Information) from the averaged prediction results, for which we expect the compounds with higher scores would show stronger activity in NCI60 dataset. We then ordered the AR antagonist scores in a descending order.

We analyzed the top 100 compounds with the highest predicted AR antagonist scores. Most of the compounds are related to the well-known anticancer drugs (NCI Drug Dictionary, DrugBank [38]), which were presented in training dataset of ToxCast and showed activity in AR-related assays. Among them are analogs of *Taxol* (*paclitaxel*) - tubulin binder, which can prevent microtubules' depolymerisation; analogs of *vinca alkaloids* (*Vimblastine*, *Vincristine*, *Vinorelbine*), which bind to the microtubular proteins of the mitotic spindle, leading to crystallization of the microtubule and mitotic arrest or cell death. We also identified analogs of *Gimatecan* and *Irinotecan* (derivatives of *camptothecin*, inhibiting the action of topoisomerase I); analogs of *Etoposide* (exhibits antitumor activity by binding to topoisomerase II); analogs of *Dactinomycin*, derived from *Streptomyces parvullus* and exhibits cytotoxic effect by reversible binding to DNA; analogs of *Trabectedin*, a marine-derived antitumor agent discovered in the *Ecteinascidia turbinata*. It binds

covalently to the minor groove of DNA, with part of the molecule interacting with nearby nuclear proteins. Another DNA intercalator, whose derivatives possess predicted AR antagonistic capacity is *Aclarubicine* (*oligosaccharide anthracycline* antibiotic isolated from the bacterium *Streptomyces galilaeus*). Another class of antibiotics was presented by analogs of *Alvespimycin* (derivative of *geldanamycin* - antineoplastic agent isolated from the bacterium *Streptomyces hygroscopicus*), mediating an antitumor activity through HSP90 inhibition. Analogs of the dye Crystal Violet were widely presented in hit list too. We also recognized analogs of fungicide agents *Pyraclostrobin* and *Trifloxystrobin* (members of the *strobilurin* group), *Triflumizole* and acaricide agent *Fenpyroximate*. The fact that most of the compounds in the top 100 list are analogs of compounds exhibiting activity in training sets is expected and reasonable.

The most interesting finding was the kinase inhibitor 1 [10], which has no direct progenitors (or analogs) in the ToxCast dataset.

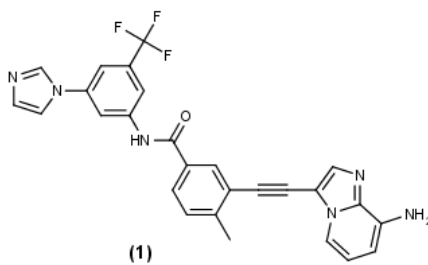


Figure 7. Compound 1

Compound 1 is reported to be an inhibitor of Breakpoint Cluster Region-Abelson kinase and its “gatekeeper” T315I mutant form, it potently inhibits proliferation of corresponding chronic myeloid leukemia Ba/F3-derived cell lines [10]. Even though further *in vitro* studies are required to prove the relevance of compound 1 as an AR antagonist, the obtained results indicate that PADME is not only capable of identifying structures sharing high similarity with training set compounds, but can also detect unobvious structural patterns and thus could serve as an instrument for drug repurposing.

4 Discussion

PADME is a very general and versatile framework, compatible with a large variety of different protein and compound featurization methods. By combining different protein descriptors like PSSM and other molecule featurization schemes like Weave [12], many more variants of PADME can be constructed, whose performances can be compared against each other. In fact, we used the Weave implementation in DeepChem as a molecular featurization method and ran hyperparameter searching on it, but the result was worse than ECFP and GraphConv, and it consumed much more time and memory than the other two, so we did not pursue it any further.

Mapping a protein into a feature vector is a task in proteochemometrics. However, most existing methods in proteochemometrics require expert knowledge and often involve 3D structural information [23,35], which is often not available. We only considered sequence information for both drugs and targets in this work to make our model more generally applicable.

It is also possible to use CNN or RNN to learn a latent feature vector to represent the proteins, based on its amino acid sequence information, instead of using fixed-rule protein descriptors like PSC as the input, so that the whole model can be trained in a completely end-to-end fashion without standalone components of the network like PSC in our implementation, making the network structure more "symmetrical". Actually, it was already attempted by Öztürk et al. [21], who showed a performance similar to PADME, but they did not use cross-validation to get average performances, they only ran different models on the same test set, which was just 1/6 the size of the whole dataset, so we think there is still much room for improvement in that direction.

We only used simple feedforward neural networks in our implementations of PADME from the Combined Input Vector to the output, but other types of Neural Networks might be able to generate better results, like Highway Networks [30], which allows the units in the network to take shortcuts, circumventing the large amounts of layers in some networks.

Pretraining also has the potential to improve our model, but we did not include it, because it might be difficult for the community to compare the real performance of PADME with other models.

Compared to previous models like SimBoost and KronRLS, PADME is not only outperforming them in terms of prediction accuracy, but is more scalable in terms of number of entities and number of prediction endpoints, because both SimBoost and KronRLS rely on similarity matrices and they are only single-task models. In the age of Big Data, this scalability will be a big advantage in virtual high-throughput screening.

5 Conclusion

To tackle DTI prediction problem from a new angle, we devised PADME framework that utilizes deep neural networks for this task. PADME incorporates both compound and target protein sequence information, so it can handle the cold-start problem, which most current deep learning-based models for DTI prediction cannot do. Predicting real-valued endpoints also makes it desirable for problems requiring finer granularity than the simple binary classification. PADME is the first to incorporate MGC with protein descriptors into the DTI prediction task, and have shown to be consistently outperforming state-of-the-art methods, but surprisingly enough, PADME based on MGC (GraphConv in our case) does not outperform PADME based on ECFP. PADME is also much more scalable than the state-of-the-art models for DTI regression task, namely SimBoost and KronRLS, and this advantage might be significant with big datasets. Another contribution is the use of the ToxCast dataset in DTI prediction problems, which we believe future research should use in addition to the other benchmarking datasets.

As a case study, we predicted the interaction strength between compounds and the androgen receptor (AR), and the compounds predicted to have strong interactions (antagonist effects) with AR tend to be analogs of active compounds in the training dataset, but some non-analog compounds are also ranked highly in the prediction. This suggests that PADME has the potential to be applied in drug development.

With the compatibility of PADME to different drug molecule and target protein featurization methods, we believe that future work could propose more PADME variants that advance the frontier of DTI prediction research.

Supporting Information

The following files are available free of charge.

- PADME_supplementary_dataset_files.zip: will be available in journal version of this paper. Exceeds size limit of arXiv.
- supplementary_text.pdf: explains data preprocessing steps and presents some additional computational experiments.

The source code and some processed dataset is deposited at <https://github.com/simonfqy/PADME>. Some bigger processed datasets could be obtained upon request.

Acknowledgments

The authors thank the help and suggestions received from our fellow lab members, including but not limited to Zaccary Alperstein, Oliver Snow, Michael Lllamosa, Fuqiang Ban, Hossein Sharifi, Beidou Wang, Jiayi Tang, Sahand Khakabimamaghani and Michael Hsing. We also express our gratitude towards our family and friends, especially Wen Xie, Qiao He, Yue Long, Aster Li, Lan Lin, Xuyan Qian, Yue Zhang, Si Chen, Fengjie Lun, Lingyun Qu and Stephen Tseng; and, most important of all, the late Mr. Xiefu Zang.

We also thank George Lucas (and his fantastic prequel trilogy) and Smith et al. [29] for the inspiration of naming.

References

1. H. Altae-Tran, B. Ramsundar, A. S. Pappu, and V. Pande. Low data drug discovery with one-shot learning. *ACS central science*, 3(4):283–293, 2017.
2. D.-S. Cao, Q.-S. Xu, and Y.-Z. Liang. propy: a tool to generate various modes of chou’s pseaac. *Bioinformatics*, 29(7):960–962, 2013.
3. G. E. Dahl, N. Jaitly, and R. Salakhutdinov. Multi-task neural networks for qsar predictions. *arXiv preprint arXiv:1406.1231*, 2014.
4. M. I. Davis, J. P. Hunt, S. Herrgard, P. Ciceri, L. M. Wodicka, G. Pallares, M. Hocker, D. K. Treiber, and P. P. Zarrinkar. Comprehensive analysis of kinase inhibitor selectivity. *Nature Biotechnology*, 29(11):1046–1051, 2011.
5. H. Ding, I. Takigawa, H. Mamitsuka, and S. Zhu. Similarity-based machine learning methods for predicting drug–target interactions: a brief review. *Briefings in Bioinformatics*, 15(5):734–747, 2014.
6. D. K. Duvenaud, D. Maclaurin, J. Iparraguirre, R. Bombarell, T. Hirzel, A. Aspuru-Guzik, and R. P. Adams. Convolutional networks on graphs for learning molecular fingerprints. In *Advances in neural information processing systems*, pages 2224–2232, 2015.

-
7. J. Gomes, B. Ramsundar, E. N. Feinberg, and V. S. Pande. Atomic convolutional networks for predicting protein-ligand binding affinity. *arXiv preprint arXiv:1703.10603*, 2017.
 8. I. Goodfellow, Y. Bengio, and A. Courville. *Deep Learning*. MIT Press, 2016. <http://www.deeplearningbook.org>.
 9. T. He, M. Heidemeyer, F. Ban, A. Cherkasov, and M. Ester. Simboost: a read-across approach for predicting drug–target binding affinities using gradient boosting machines. *Journal of Cheminformatics*, 9(1):24, 2017.
 10. W.-S. Huang, C. A. Metcalf, R. Sundaramoorthi, Y. Wang, D. Zou, R. M. Thomas, X. Zhu, L. Cai, D. Wen, S. Liu, et al. Discovery of 3-[2-(imidazo [1, 2-b] pyridazin-3-yl) ethynyl]-4-methyl-n-{4-[(4-methylpiperazin-1-yl) methyl]-3-(trifluoromethyl) phenyl} benzamide (ap24534), a potent, orally active pan-inhibitor of breakpoint cluster region-abelson (bcr-abl) kinase including the t315i gatekeeper mutant. *Journal of medicinal chemistry*, 53(12):4701–4719, 2010.
 11. J. Jimenez. pygpgo: Bayesian optimization for python.
 12. S. Kearnes, K. McCloskey, M. Berndl, V. Pande, and P. Riley. Molecular graph convolutions: moving beyond fingerprints. *Journal of computer-aided molecular design*, 30(8):595–608, 2016.
 13. D. P. Kingma and J. Ba. Adam: A method for stochastic optimization. *arXiv preprint arXiv:1412.6980*, 2014.
 14. G. Landrum. Rdkit: Open-source cheminformatics.
 15. Y. LeCun, Y. Bengio, and G. Hinton. Deep learning. *nature*, 521(7553):436–444, 2015.
 16. J. Ma, R. P. Sheridan, A. Liaw, G. E. Dahl, and V. Svetnik. Deep neural nets as a method for quantitative structure–activity relationships. *Journal of chemical information and modeling*, 55(2):263–274, 2015.
 17. A. Mayr, G. Klambauer, T. Unterthiner, and S. Hochreiter. Deeptox: toxicity prediction using deep learning. *Frontiers in Environmental Science*, 3:80, 2016.
 18. J. T. Metz, E. F. Johnson, N. B. Soni, P. J. Merta, L. Kifle, and P. J. Hajduk. Navigating the kinome. *Nature chemical biology*, 7(4):200, 2011.
 19. A. Mina, R. Yoder, and P. Sharma. Targeting the androgen receptor in triple-negative breast cancer: current perspectives. *OncoTargets and therapy*, 10:4675, 2017.
 20. Z. Mousavian, S. Khakabimamaghani, K. Kavousi, and A. Masoudi-Nejad. Drug–target interaction prediction from pssm based evolutionary information. *Journal of pharmacological and toxicological methods*, 78:42–51, 2016.
 21. H. Öztürk, E. Ozkirimli, and A. Özgür. Deepdta: Deep drug-target binding affinity prediction. *arXiv preprint arXiv:1801.10193*, 2018.

-
22. T. Pahikkala, A. Airola, S. Pietilä, S. Shakyawar, A. Sz wajda, J. Tang, and T. Aittokallio. Toward more realistic drug–target interaction predictions. *Briefings in bioinformatics*, 16(2):325–337, 2014.
 23. T. Qiu, J. Qiu, J. Feng, D. Wu, Y. Yang, K. Tang, Z. Cao, and R. Zhu. The recent progress in proteochemometric modelling: focusing on target descriptors, cross-term descriptors and application scope. *Briefings in bioinformatics*, page bbw004, 2016.
 24. D. Rogers and M. Hahn. Extended-connectivity fingerprints. *Journal of chemical information and modeling*, 50(5):742–754, 2010.
 25. J. Schmidhuber. Deep learning in neural networks: An overview. *Neural networks*, 61:85–117, 2015.
 26. B. Shahriari, K. Swersky, Z. Wang, R. P. Adams, and N. De Freitas. Taking the human out of the loop: A review of bayesian optimization. *Proceedings of the IEEE*, 104(1):148–175, 2016.
 27. A. Sharma, J. Lyons, A. Dehzangi, and K. K. Paliwal. A feature extraction technique using bi-gram probabilities of position specific scoring matrix for protein fold recognition. *Journal of theoretical biology*, 320:41–46, 2013.
 28. R. H. Shoemaker. The nci60 human tumour cell line anticancer drug screen. *Nature Reviews Cancer*, 6(10):813–823, 2006.
 29. J. S. Smith, O. Isayev, and A. E. Roitberg. Ani-1: an extensible neural network potential with dft accuracy at force field computational cost. *Chemical science*, 8(4):3192–3203, 2017.
 30. R. K. Srivastava, K. Greff, and J. Schmidhuber. Highway networks. *arXiv preprint arXiv:1505.00387*, 2015.
 31. J. Tang, A. Sz wajda, S. Shakyawar, T. Xu, P. Hintsanen, K. Wennerberg, and T. Aittokallio. Making sense of large-scale kinase inhibitor bioactivity data sets: a comparative and integrative analysis. *Journal of Chemical Information and Modeling*, 54(3):735–743, 2014.
 32. T. Unterthiner, A. Mayr, G. Klambauer, M. Steijaert, J. K. Wegner, H. Ceulemans, and S. Hochreiter. Multi-task deep networks for drug target prediction. In *Neural Information Processing System*, pages 1–4, 2014.
 33. E. US. Toxcast summary files from invitrodb_v2. <https://www.epa.gov/chemical-research/toxicity-forecaster-toxcasttm-data>, 10 2015. Accessed: 2018-03-22.
 34. E. US. Toxicity forecaster (toxcast) fact sheet. https://www.epa.gov/sites/production/files/2016-12/documents/tox_cast_fact_sheet_dec2016.pdf, 2016. Accessed: 2018-03-22.
 35. G. J. van Westen, J. K. Wegner, A. P. IJzerman, H. W. van Vlijmen, and A. Bender. Proteochemometric modeling as a tool to design selective compounds and for extrapolating to novel targets. *MedChemComm*, 2(1):16–30, 2011.
-

-
36. I. Wallach, M. Dzamba, and A. Heifets. Atomnet: A deep convolutional neural network for bioactivity prediction in structure-based drug discovery. *arXiv preprint arXiv:1510.02855*, 2015.
 37. M. Wen, Z. Zhang, S. Niu, H. Sha, R. Yang, Y. Yun, and H. Lu. Deep-learning-based drug-target interaction prediction. *Journal of proteome research*, 16(4):1401–1409, 2017.
 38. D. S. Wishart, Y. D. Feunang, A. C. Guo, E. J. Lo, A. Marcu, J. R. Grant, T. Sajed, D. Johnson, C. Li, Z. Sayeeda, et al. Drugbank 5.0: a major update to the drugbank database for 2018. *Nucleic acids research*, 46(D1):D1074–D1082, 2017.
 39. Z. Wu, B. Ramsundar, E. N. Feinberg, J. Gomes, C. Geniesse, A. S. Pappu, K. Leswing, and V. Pande. Moleculenet: a benchmark for molecular machine learning. *Chemical science*, 9(2):513–530, 2018.
 40. Y. Yamanishi, M. Araki, A. Gutteridge, W. Honda, and M. Kanehisa. Prediction of drug-target interaction networks from the integration of chemical and genomic spaces. *Bioinformatics*, 24(13):232–240, 2008.
 41. T. A. Yap, A. D. Smith, R. Ferraldeschi, B. Al-Lazikani, P. Workman, and J. S. de Bono. Drug discovery in advanced prostate cancer: translating biology into therapy. *Nature Reviews Drug Discovery*, 15(10):699, 2016.
 42. 徐优俊 and 裴剑锋. 深度学习在化学信息学中的应用. *大数据*, 3(2):2017019, 2017.